15th IFK
Proc. of the 15th International Fluid Power Conference <Symposium/Conference>
<DOI>

Analysis of High-Pressure Pneumatic Stage Separation System for Reusable Launch Vehicles Based on Real Gas Equation of State

Ruiyao Tao[1], Yaobao Yin[1,2*], Naiping Gao[1], Pengfei He[3]

[1] *School of Mechanical Engineering, Tongji University,Shanghai,201804, P.R.China*
[2] *Shanghai Key Laboratory of Wearable Robotics and Human-Robot Interaction Technology, Shanghai 201804, P.R.China*
[3] *School of Aerospace Engineering and Applied Mechanics, Shanghai, 200082, P.R.China*

Corresponding author: y-yin@tongji.edu.cn

Abstract.

Interstage separation of launch vehicles is essential for reliable payload delivery into orbit. Helium, owing to its chemical inertness and low density, is widely used as the working medium in pneumatic separation systems. While high-pressure helium deviates significantly from ideal-gas behavior, and traditional cubic equations of state (EoS) introduce cumulative errors. To overcome these issues, a new corresponding state EoS is proposed, considering intermolecular interactions and the influence of temperature on molecular forces and volume. Based on the new EoS, a transient thermodynamic model is established, with strategies developed for both open and closed systems, and applied to the analysis of interstage separation. Results indicate that within –30 °C to 120 °C and 1–35 MPa, the proposed EoS achieves a maximum absolute error below 0.82%, significantly improving computational accuracy. The transient model reproduces the thermodynamic behavior of fixed-volume open, variable-volume open, and variable-volume closed systems, with average deviations from experiments below 5.2%, confirming its validity. Under heavy-load conditions of 90 t and 120 t, the minimum supply pressure of the gas tank is determined to be 12.5 MPa to ensure a separation velocity ≥ 5 m/s while keeping the separation duration under 1000 ms. A theoretical basis and key parameters are provided for the design and optimization of interstage separation systems.

Keywords. Real-gas equation of state, Helium, Interstage separation, Launch vehicles, Transient thermodynamic modelling.

1. INTRODUCTION

During the flight of a launch vehicle, multiple separation events are required, among which the interstage separation system plays a crucial role in reducing structural mass and improving payload efficiency, as shown in Figure. 1. The primary task of this system is to achieve non-interfering separation of the expended stage within a millisecond timescale [1]. This process involves precise mechanisms that must be triggered at the exact moment while minimizing disturbances to the attitude and trajectory of vehicle.

Currently, two main technical approaches are employed for interstage separation. Traditional expendable configurations predominantly rely on pyrotechnic devices, in which energetic materials drive the separation mechanism by breaking or releasing structural connections between stages [2]. In contrast, non-pyrotechnic separation technologies significantly reduce the adverse effects of high temperature and explosive shock, offering greater flexibility and enabling safe separation under low-thermal-load conditions [3]. Typical non-pyrotechnic approaches include mechanical separation [4], electromechanical separation [5], electromagnetic separation, smart-material–driven separation [6], and pneumatic separation [7]. Among these, pneumatic separation is the most widely applied owing to its advantages of reusability, versatility, and low cost [8]. This technique relies solely on compressed gas to generate thrust, thereby enabling the relative acceleration between adjacent stages.

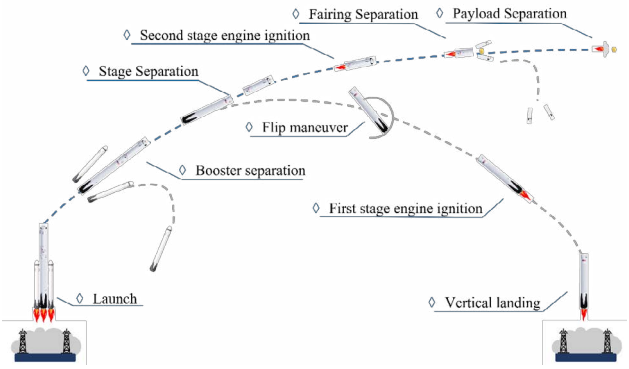

Figure 1.1 Multiple Separation Events of a Launch Vehicle

For safety considerations, helium is commonly selected as the working medium in pneumatic separation systems, primarily due to its chemical inertness and low specific gravity [9]. The molar mass of helium is only one-seventh that of air, which enables a significant reduction in the volume and weight of storage vessels while meeting system performance requirements. Consequently, the structural mass of the launch vehicle can be lowered, and the required amount of pressurant for a given structural configuration can be reduced, thereby further decreasing overall energy consumption. In high-pressure helium systems used for rocket interstage separation, the working fluid often exists under high-pressure or even supercritical conditions. Under such circumstances, the ideal gas law fails to accurately capture the thermodynamic behavior, making the development of an equation of state (EoS) capable of representing real-gas effects particularly essential [10].

Among existing formulations, cubic EoS, typified by the van der Waals (VDW) EoS [11], have attracted considerable attention in both engineering practice and scientific research. To improve accuracy in representing vapor-phase behavior, Redlich and Kwong [12] modified the temperature-dependent term of the VDW EoS. Building on this foundation, Soave [13] and Peng and Robinson [14] introduced further refinements to the temperature and volume functions, resulting in the SRK and PR EoSs, respectively, which significantly enhanced the predictive accuracy of pure substances over a wider temperature range and under vapor–liquid equilibrium conditions. Alternatively, virial-type EoS, expressed as a power series expansion, exhibit reliable predictive performance in the low-pressure region [15].

Extensions to this class of EoS have been achieved by introducing empirical parameters, as demonstrated by Benedict, Webb, and Rubin, and subsequently by Lee et al. [16], thereby broadening their applicability to multicomponent mixtures.

With the advancement of statistical mechanics and computational science, the focus of EoS research has gradually shifted toward theoretical formulations rooted in molecular interaction mechanisms. Based on perturbation theory, Chapman et al. [17] developed the Statistical Associating Fluid Theory (SAFT), which incorporates successive contributions of intermolecular interactions and provides accurate descriptions of complex fluid behavior. Building upon this framework, Alanazi et al. [18] introduced thermodynamic models that account for chain structures and molecular association phenomena, and compared them with cubic EoS for hydrogen-containing mixtures. Their results indicated that cubic EoS retain superior predictive performance for such systems. Despite their sound physical foundation, EoS derived from perturbation theory and virial coefficients are computationally intensive and exhibit limitations in predicting thermophysical properties under high-pressure conditions.

To address these issues, a new real-gas EoS is proposed by combining the advantages of cubic formulations and perturbation theory. Through the introduction of composite molecular correction factors and temperature-dependent coefficients, the accuracy of helium property prediction under high-pressure conditions is significantly improved. On this basis, a transient thermodynamic system model incorporating real-gas effects is established to capture the dynamic variations of pressure and temperature within the interstage separation chamber. Finally, the validity of the proposed model is verified through a case study of a high-pressure helium separation system for rocket interstages, providing critical theoretical insights and technical parameters for the design of aerospace separation systems.

2. Real-Gas Equation of State Applicable to High-Pressure Helium Systems

When analyzing high-pressure helium systems, the choice of an appropriate EoS is essential for accurately predicting the physical properties of the gas. Helium, an inert gas with a stable closed-shell electronic structure, is a monoatomic and nonpolar species characterized by a symmetric electron cloud. Moreover, due to its very low molecular weight, helium exhibits pronounced quantum effects and is regarded as a prototypical quantum gas.

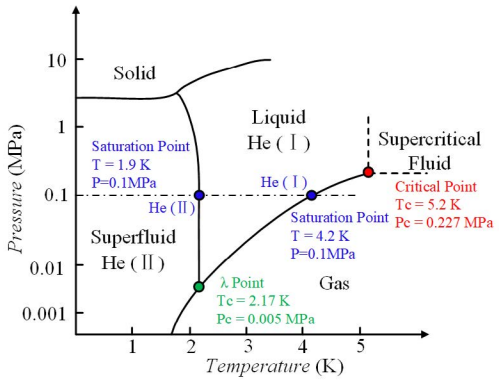

Figure 2.1. Phase Diagram of Helium

As shown in Figure. 2.1, the phase diagram of helium is unique in that it exhibits two liquid phases: the normal liquid phase (He I) and the superfluid phase (He II). Consequently, helium does not possess a conventional solid–liquid–vapor triple point. Instead, a λ-point appears at the intersection of the vapor, liquid, and superfluid phases.

The ideal-gas EoS assumes that gas molecules are point masses without volume and that no intermolecular forces exist other than elastic collisions. In reality, helium is a quantum system with intermolecular interactions, and its behavior deviates substantially from the classical ideal model of non-interacting point particles. This deviation becomes particularly significant under high-pressure conditions, where the weak but non-negligible dispersion forces arising from its nonpolarity and inertness become increasingly important, and the finite molecular volume is more pronounced. Under such circumstances, the ideal-gas EoS fails to provide accurate predictions, and the adoption of a real-gas EoS is therefore indispensable.

2.1. Real-Gas Equation of State

Common real-gas EoS can be classified from several perspectives, as summarized in Table 2.1. Virial-type EoS involve complicated mathematical expressions, multiparameter EoS are

Table 2.1. Types of Commonly Used Real Gas EoS

Type	Theoretical basis	Representative equations
Virial	Statistical mechanics	$p = RT\rho(1 + B\rho + C\rho^2 + D\rho^3 + \cdots)$
Cubic	Van der Waals concept	Van der Waals EoS: $p = \frac{RT}{V_m - b} - \frac{a}{V_m^2}$ Redlich-Kwong EoS: $p = \frac{RT}{V_m - b} - \frac{a}{T^{0.5}V_m(V_m + b)}$ Soave-Redlich-Kwong EoS: $p = \frac{RT}{V_m - b} - \frac{a(T)}{V_m(V_m + b)}$ Peng-Robinson EoS: $p = \frac{RT}{V_m - b} - \frac{a(T)}{V_m(V_m + b) + b(V_m - b)}$
Multiparameter	Empirical fitting	Benedict-Webb-Rubin EoS: $p = RT\rho + (B_0RT - A_0 - C_0/T^2)\rho^2 + (bRT - a)\rho^3 + a\alpha\rho^6 + C\rho^3/T^2\,(1 + \gamma\rho^2)e^{-\gamma\rho^2}$
Perturbed-chain	Statistical mechanics	Statistical associating fluid theory: $A^{total} = A^{idealgas} + A^{monomer} + A^{chain} + A^{association} + A^{other}$
Crossover	Scaling laws	Universal method [19]: $p = -\left(\frac{\partial A}{\partial v}\right)_T = \frac{RT}{v_{0c}}\left[-\frac{v_{0c}}{v_c}\left(\frac{\partial \Delta\bar{A}}{\partial \Delta\eta}\right)_T + \left(\frac{1}{b} - \frac{T_{0c}}{T}\frac{\Omega_a a_0}{Z_{0c}b_2b_3}\right) + \frac{v_{0c}}{v_c}\left(\frac{\partial K}{\partial \Delta\eta}\right)_T\right]$

strongly dependent on experimental data, and perturbation-chain or crossover-type EoS are suitable for describing complex molecular systems. By contrast, cubic EoS require fewer parameters and involve simpler calculations, making them more applicable for analyzing high-pressure helium systems.

The compressibility factor Z is an important dimensionless parameter that characterizes the deviation of real gases from ideal-gas behavior, defined as

$$Z(p,T) = \frac{pV_m}{RT} \tag{2.1}$$

For an ideal gas, Z is always equal to 1. In the case of real gases, however, Z is a function of both pressure and temperature, reflecting the influence of intermolecular interactions. For helium, the compressibility factor varies with both pressure and temperature.

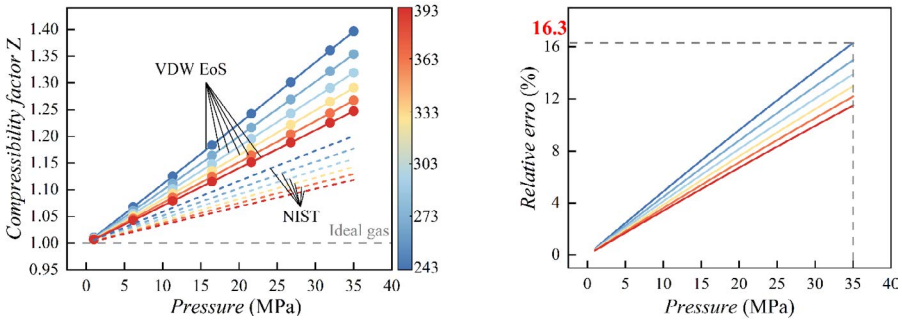

(a) Compressibility factor Z comparison (b) Absolute error in Z

Figure 2.2. Prediction Accuracy of VDW EoS: Comparison with NIST Data

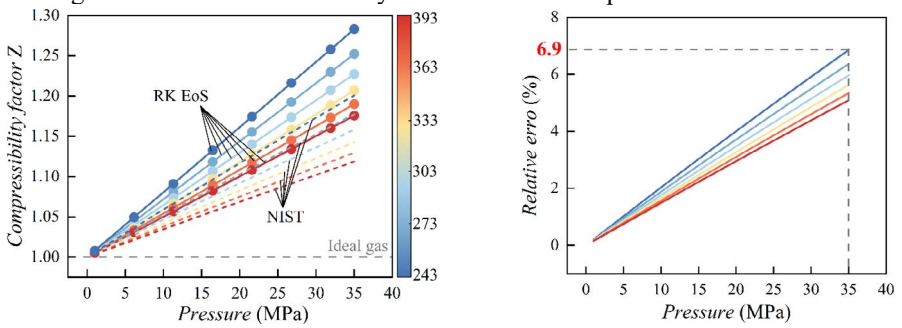

(a) Compressibility factor Z comparison (b) Absolute error in Z

Figure 2.3. Prediction Accuracy of RK EoS: Comparison with NIST Data

The variation of the compressibility factor of helium with pressure and temperature is investigated. To assess the predictive accuracy of classical cubic EoS, four representative EoSs are selected: van der Waals (VDW), Redlich–Kwong (RK), Soave–Redlich–Kwong (SRK), and Peng–Robinson (PR) EoSs. The compressibility factors of helium are calculated using these formulations and compared systematically with the reference data from the REFPROP database developed by the National Institute of Standards and Technology (NIST). The results are presented in Figures 2.2–2.5.

The comparison shows that within the typical operating range of high-pressure helium systems for interstage separation, with temperatures from 243 K to 393 K (−30 °C to 120

°C) and pressures from 1 MPa to 35 MPa, the VDW EoS exhibits the largest absolute error of 16.3%. The errors for the RK and PR EoSs are 6.9% and −4.1%, respectively, whereas the SRK EoS yields the smallest deviation of 2.5%. It should be noted that due to inherent assumptions and simplifications in the EoSs, systematic deviations arise in the prediction of high-pressure helium properties. Such deviations may further accumulate in practical engineering modeling. Therefore, in order to improve the accuracy of high-pressure helium system calculations, it is necessary to employ a real-gas EoS with smaller intrinsic prediction errors.

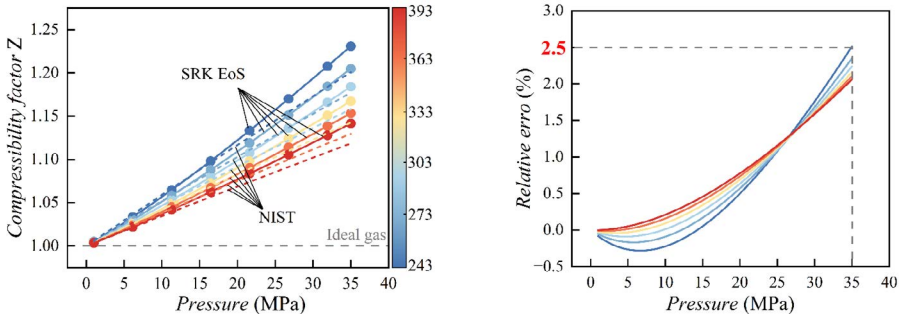

(a) Compressibility factor Z comparison (b) Absolute error in Z

Figure 2.4. Prediction Accuracy of SRK EoS: Comparison with NIST Data

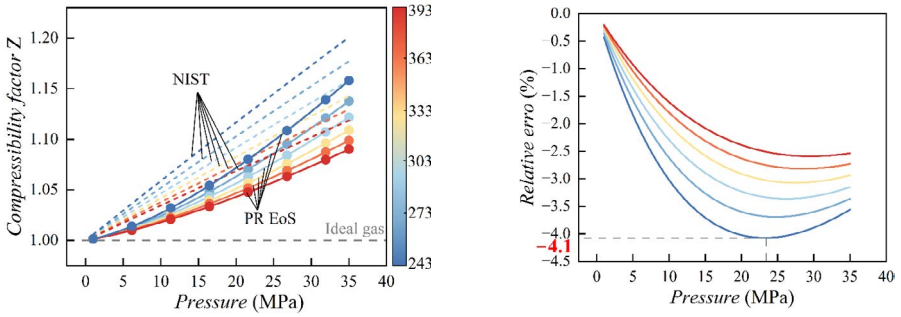

(a) Compressibility factor Z comparison (b) Absolute error in Z

Figure 2.5. Prediction Accuracy of PR EoS: Comparison with NIST Data

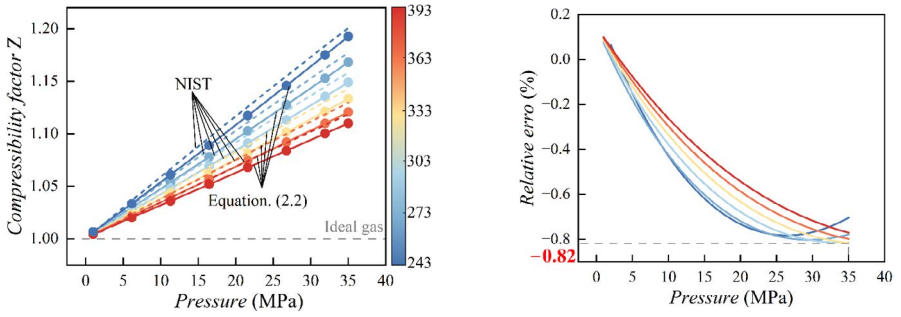

(a) Compressibility factor Z comparison (b) Absolute error in Z

Figure 2.6. Prediction Accuracy of (2.2) EoS: Comparison with NIST Data

2.2. A New Real-Gas Corresponding State EoS

By combining the advantages of cubic EoS and perturbation theory, and considering the molecular association phenomena under high-pressure conditions, a new real-gas corresponding state EoS is developed based on statistical thermodynamics. The specific form of the equation is expressed as follows [20]:

$$p_r = \frac{8}{3}\left[\frac{T_r}{V_{mr}/\gamma - \xi/3} - \frac{9/8}{T_r^{\alpha}(V_{mr}/\gamma)^2}\right] \tag{2.2}$$

According to the principles of statistical thermodynamics, a composite molecular correction factor is introduced to represent the ratio between the actual number of molecules N_t contained in 1 kg of gas under arbitrary states and the number of molecules N_c under the critical state:

$$\gamma = \frac{N_t}{N_c} = \left(\frac{3}{8Z_c}\right) \cdot \left[1 - \left(1 - \frac{8}{3}Z_c\right) \cdot T_r^{-\Delta I/2} \cdot e^{(1/T_r - 1)} \cdot V_r^{-1}\right] \tag{2.3}$$

In addition, the effects of temperature on molecular volume and intermolecular forces are taken into account. The resulting molecular volume correction coefficient is given as:

$$\xi = \frac{b}{b_c} = \sqrt{\frac{0.5 + \sqrt{0.25 + 0.375}}{0.5 + \sqrt{0.25 + 0.375T_r}}} \tag{2.4}$$

And the intermolecular force correction coefficient is expressed as:

$$\alpha = \left[\ln\left(\frac{27}{8}\right) - \ln\sqrt{\frac{0.5 + \sqrt{0.25 + 0.375}}{0.5 + \sqrt{0.25 + 0.375\,T_B/T_c}}}\right] \Big/ \ln(T_B/T_c) - 1 \tag{2.5}$$

Within the same ranges of temperature and pressure, calculations are performed using Equation (2.2), and the predicted values are systematically compared with reference data from the NIST database. The absolute error distribution is also plotted, as shown in Figure 2.6. The results indicate that the maximum absolute error of the proposed EoS is only 0.82%, demonstrating high predictive accuracy. Furthermore, the proposed formulation is concise in form and clear in structure, which facilitates its practical application in engineering systems.

3. HIGH-PRESSURE GAS ANALYSIS METHOD BASED ON A REAL-GAS EOS

High-pressure helium thermodynamic systems can generally be categorized into open and closed systems, as illustrated in Figure 3.1. An open system allows both mass and energy exchange with the surroundings, whereas a closed system permits only energy exchange without mass transfer. When formulating the thermodynamic conservation equations for high-pressure helium systems, pressure and temperature are adopted as the primary variables to characterize mass and energy conservation. Based on the first law of thermodynamics and incorporating the real-gas equation of state, time-dependent governing equations are derived with pressure and temperature as state variables. This provides the foundation for transient analysis of the system.

3.1. Thermodynamic Model of Open System

The real-gas equation of state in Equation (2.2) can be expressed as:

$$f(m,p,V,T) = 0 \tag{3.1}$$

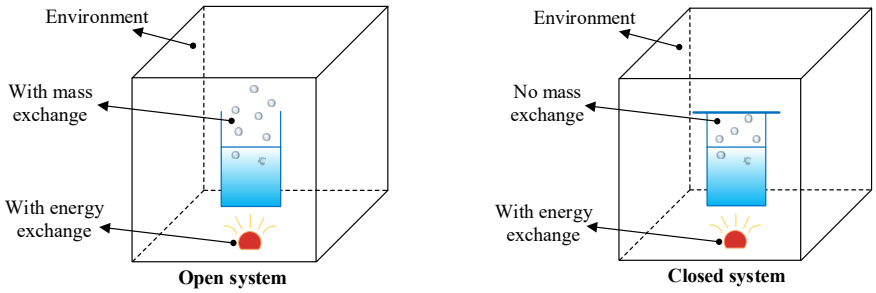

(a) Open system (b) Closed system

Figure 3.1. Mass and Energy Exchange in Open and Closed Thermodynamic Systems

Assuming gas pressure, mass, temperature, and volume are taken as variables, the partial differential form is obtained. Accordingly, the time-dependent variations of pressure, mass, temperature, and volume can be written as:

$$\frac{\partial f}{\partial p}\frac{\mathrm{d}p}{\mathrm{d}t} + \frac{\partial f}{\partial m}\frac{\mathrm{d}m}{\mathrm{d}t} + \frac{\partial f}{\partial T}\frac{\mathrm{d}T}{\mathrm{d}t} + \frac{\partial f}{\partial V}\frac{\mathrm{d}V}{\mathrm{d}t} = 0 \tag{3.2}$$

From this relation, the governing equation with pressure as the primary variable is derived as:

$$\frac{\mathrm{d}p}{\mathrm{d}t} = -\frac{\partial f}{\partial m}\frac{\mathrm{d}m}{\mathrm{d}t} - \frac{\partial f}{\partial T}\frac{\mathrm{d}T}{\mathrm{d}t} - \frac{\partial f}{\partial V}\frac{\mathrm{d}V}{\mathrm{d}t} \tag{3.3}$$

(a) Typical fixed-volume open system (b) Typical variable-volume open system

Figure 3.2. Typical Open Systems

Figure 3.3. Typical Closed Systems

The gas inside the high-pressure chamber follows the first law of thermodynamics, where the increment of system energy equals the difference between the input and output energy. This is expressed as:

$$\mathrm{d}U + \delta E_k + \delta E_p = h_{in}\mathrm{d}m_{in} - h_{out}\mathrm{d}m_{out} + \delta Q - \delta W \tag{3.4}$$

Combined with the second law of thermodynamics, the internal energy can be formulated as a function of any two independent variables among T, p, and v. Expressed in terms of T and v., the first internal energy equation is given by:

$$\mathrm{d}u = c_v \mathrm{d}T + \left[T\left(\frac{\partial p}{\partial T}\right) - p\right] dv \tag{3.5}$$

For fixed-volume open systems such as gas cylinders, shown in Figure 3.2(a), the system performs no external work, and only a single inlet or outlet exists for the gas. Neglecting changes in kinetic and potential energy, the first law of thermodynamics for a fixed-volume open system is expressed as:

$$u\mathrm{d}m + m\mathrm{d}u = (u + pv)\mathrm{d}m + \delta Q \tag{3.6}$$

By substituting Equation (3.5) into Equation (3.6), the time-dependent governing equation for temperature in a fixed-volume open system is obtained as:

$$\mathrm{d}T = \frac{1}{mc_v}\left[T\left(\frac{\partial p}{\partial T}\right)\right]\left(\frac{V}{m}\right)\mathrm{d}m + \frac{\delta Q}{mc_v} \tag{3.7}$$

where the partial derivative of pressure with respect to temperature is evaluated based on the real-gas EoS in Equation (2.2).

Due to the constant volume of the open system, the time-dependent pressure governing equation is given by Equation (3.3):

$$\frac{\mathrm{d}p}{\mathrm{d}t} = -\frac{\partial f}{\partial m}\frac{\mathrm{d}m}{\mathrm{d}t} - \frac{\partial f}{\partial T}\frac{\mathrm{d}T}{\mathrm{d}t} \tag{3.8}$$

For variable-volume open systems, such as the rodless chamber of an intake cylinder shown in Figure 3.2(b), and by neglecting changes in gas kinetic and potential energy, the first law of thermodynamics is expressed as:

$$u\mathrm{d}m + m\mathrm{d}u = (u_{in} + pv_{in})\mathrm{d}m + \delta Q - p\mathrm{d}V \tag{3.9}$$

By substituting Equation (3.5) into Equation (3.9), the time-dependent governing equation for temperature in a variable-volume open system is obtained as:

$$\mathrm{d}T = \frac{1}{mc_v}(u_{in} - u)\mathrm{d}m + \frac{1}{mc_v}\left[T\left(\frac{\partial p}{\partial T}\right)\right]\left(\frac{V}{m}\right)\mathrm{d}m - \frac{1}{mc_v}\left[T\left(\frac{\partial p}{\partial T}\right)\right]\mathrm{d}V + \frac{\delta Q}{mc_v} \tag{3.10}$$

where the variation of specific internal energy is derived by integrating Equation (3.5), which yields:

$$u_{in} - u = \int c_v \mathrm{d}T + \int \left[T\left(\frac{\partial p}{\partial T}\right) - p\right] dv \tag{3.11}$$

The time-dependent governing equation for pressure in a variable-volume open system is obtained as Equation (3.3).

3.2. Thermodynamic model of closed systems

For variable-volume closed systems, such as the rod chamber of a cylinder shown in Figure 3.3, the gas volume, temperature, and pressure vary with time, while the mass remains constant. By neglecting changes in gas kinetic and potential energy, the first law of thermodynamics is expressed as:

$$m\mathrm{d}u = -p\mathrm{d}V + \delta Q \tag{3.12}$$

By substituting Equation (3.5) into Equation (3.12), the time-dependent governing equation for temperature in a variable-volume closed system is obtained as:

$$\mathrm{d}T = -\frac{1}{mc_v}\left[T\left(\frac{\partial p}{\partial T}\right)\right]\mathrm{d}V + \frac{\delta Q}{mc_v} \tag{3.13}$$

Since the mass of a variable-volume closed system remains constant, its time-dependent governing equation for pressure is derived from Equation (3.3) as:

$$\frac{\mathrm{d}p}{\mathrm{d}t} = -\frac{\partial f}{\partial T}\frac{\mathrm{d}T}{\mathrm{d}t} - \frac{\partial f}{\partial V}\frac{\mathrm{d}V}{\mathrm{d}t} \tag{3.14}$$

By solving the governing equations of pressure and temperature for the three typical thermodynamic systems, a transient thermodynamic system model that incorporates real-gas effects is established.

4. THEORETICAL ANALYSIS AND EXPERIMENTAL VALIDATION OF THE INTERSTAGE PNEUMATIC SEPARATION SYSTEM

The investigated interstage pneumatic separation system consists of four high-pressure supply gas tanks connected in series, solenoid valve, and a separation cylinder, as shown in Figure 4.1. Before system operation, the gas tanks are pre-charged with high-pressure helium as the energy source. Upon receiving the activation command, allowing the high-pressure gas to pass through the valve and flow into the rodless chamber of the separation cylinder. The piston is then driven to move, generating the thrust required for separation and enabling the rapid unlocking and separation of the first and second stages, as illustrated in Figure 4.2.

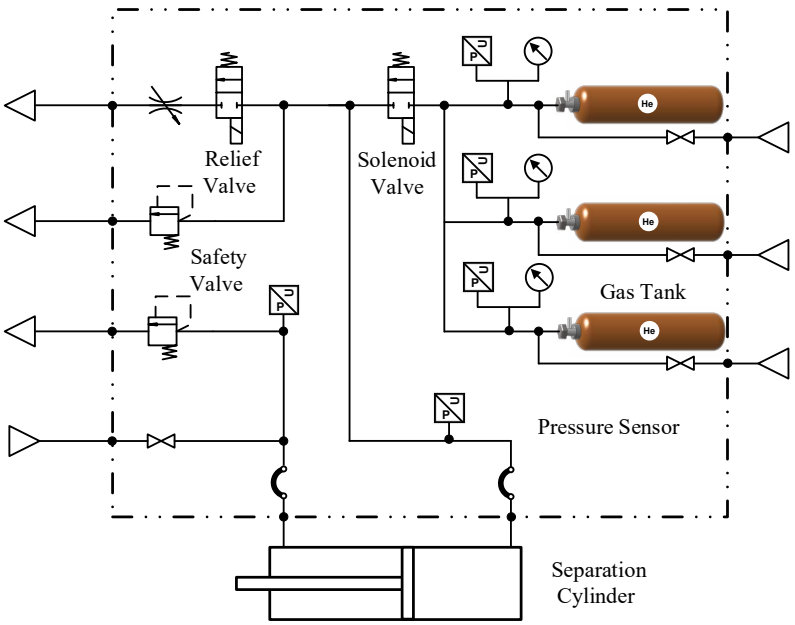

Figure 4.1 Schematic diagram of the interstage high-pressure helium separation system

For the first stage of the rocket, which is connected to the cylinder barrel, the force balance equation is expressed as:

$$p_1 A_1 - p_2 A_2 = m_1 \frac{\mathrm{d}^2 x_1}{\mathrm{d}t^2} + B_1 \frac{\mathrm{d}x_1}{\mathrm{d}t} + K_1 x_1 - \beta m_1 g \tag{4.1}$$

For the second stage, which is connected to the piston rod, the force balance equation is expressed as:

$$p_1 A_1 - p_2 A_2 = m_2 \frac{\mathrm{d}^2 x_2}{\mathrm{d}t^2} + B_2 \frac{\mathrm{d}x_2}{\mathrm{d}t} + K_2 x_2 - \beta m_2 g \tag{4.2}$$

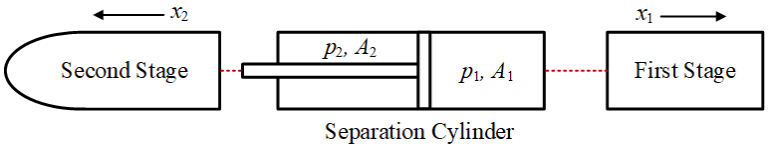

Figure 4.2 Connection relationship between the stages and the separation cylinder [21]

Table 4.1. Calculation Parameters and Values

Parameter	Symbol/Unit	Value
Critical pressure of helium	p_c/MPa	0.227
Critical temperature of helium	T_c/K	5.2
Critical volume of helium	V_{mc}/(m^3/mol)	57.3e-6
Molar mass of helium	M/(kg/mol)	4.003e-3
Gas cylinder volume	V/L	80
First-stage mass	m_1/t	90
Second-stage mass	m_2/t	120
Gravitational acceleration	g/(m/s^2)	9.8

To simulate the dynamic characteristics of the high-pressure chambers in this pneumatic system, a high-pressure gas analysis method based on a real-gas EoS is employed. According to the thermodynamic characteristics of the system components, the high-pressure gas tank is treated as a fixed-volume open system, with its pressure and temperature dynamics governed by Equations (3.7) and (3.8). The rodless chamber of the cylinder is treated as a variable-volume open system, described by Equations (3.10) and (3.3). The rod chamber is modeled as a variable-volume closed system, with pressure and temperature variations governed by Equations (3.13) and (3.14). Together, these equations establish a complete mathematical model for the system's dynamic response. The differential equations are solved using an eighth-order Dormand–Prince algorithm, with relevant constant parameters listed in Table 2, where load conditions are referenced to a representative heavy-lift rocket stage of approximately 100 t as reported by NASA [22]. Since the interstage separation process occurs on a millisecond time scale, which is much shorter than the characteristic timescale of heat transfer, the system is treated as adiabatic.

During the construction of the ground test bench for interstage separation, the first and second stages are simulated by coaxially arranged rail-mounted flat cars. Pressure sensors are installed in the gas supply system to monitor the pressures in the gas tank, the rodless chamber, and the rod chamber of the actuator cylinder. The supply pressure during the test

is 13.2 MPa. The separation instant is defined as the moment when the first and second stages just lose contact, which is measured to occur at 967 ms. A comparison between the theoretical model and the experimental results shows that the average percentage errors of the three chambers are 1.62%, 3.15%, and 5.14%, respectively, thereby validating the accuracy of the theoretical model. The comparison of pressure characteristics between theoretical predictions and experimental results, as well as the theoretical temperature variation curve, is presented in Figure 4.3.

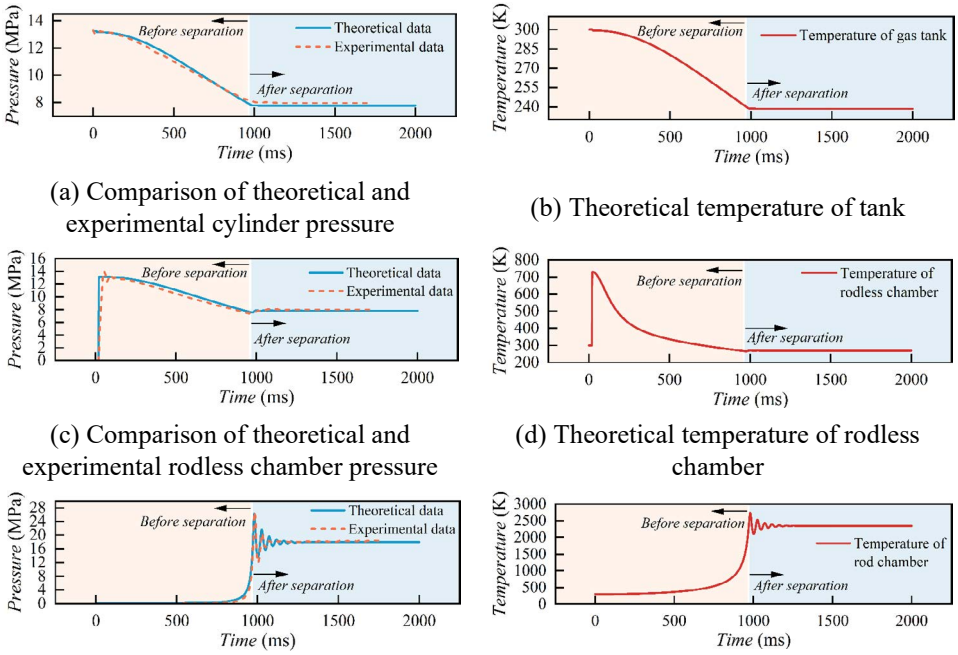

(a) Comparison of theoretical and experimental cylinder pressure

(b) Theoretical temperature of tank

(c) Comparison of theoretical and experimental rodless chamber pressure

(d) Theoretical temperature of rodless chamber

(e) Comparison of theoretical and experimental rod chamber pressure

(f) Theoretical temperature of rod chamber

Figure 4.3. Comparison of Theoretical and Experimental Results for Interstage Separation Pressure Characteristics and Theoretical Temperature Profile

After the separation command is issued, the gas tanks begin supplying the rodless chamber through the solenoid valves. The pressure evolution during separation can be divided into three stages:

(1) Before separation: The pressure in the gas tanks decreases gradually (Figure 4.3(a)), while the rodless chamber pressure rises rapidly until it matches the tank pressure (Figure 4.3(c)). Once the rodless chamber pressure exceeds the piston start-up pressure, the piston rod begins to extend, leading to an increase in chamber volume and a gradual decrease in pressure.

(2) At the separation point: The piston rod reaches its maximum displacement, and the rodless chamber volume stabilizes. At this moment, the gas tanks and rodless chamber are fully connected, maintaining equal pressures. Meanwhile, the volume of the rod chamber reaches its minimum, and its internal pressure rises sharply to a peak value (Figure 4.3(e)).

(3) After separation: The cylinder system can be abstracted as a mass–spring system under inertial effects. Due to gas compressibility, the piston rod undergoes oscillatory motion, which gradually decays to an equilibrium state.

The gas temperature variations in each chamber follow a similar trend to the pressure changes, as shown in Figure 4.3(b), (d), (f), consistent with fundamental thermodynamic principles.

The fundamental task of the interstage separation system is to achieve reliable separation of the two stages within an extremely short time and over a limited stroke. The relative separation velocity serves as the most direct indicator of this function. As shown in Figure 4.4(a), at the moment of separation, the relative velocity reaches a maximum of 5.52 m/s. A higher separation velocity indicates a faster separation action. As illustrated in Figure 4.4(b), with increasing inlet pressure, the separation velocity increases accordingly, and the time required to reach the maximum velocity is shortened. To ensure that the separation velocity is not lower than 5 m/s and that the separation duration is less than 1000 ms, the minimum supply pressure of the gas tank must be no less than 12.5 MPa.

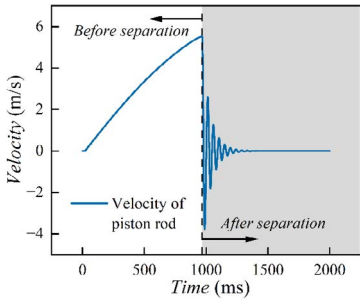

(a) Velocity of the separation cylinder piston rod

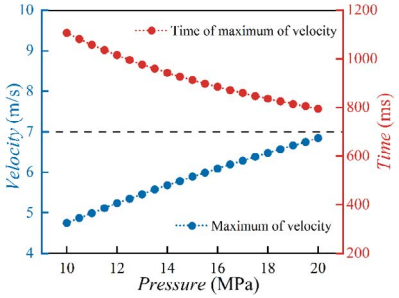

(b) Separation velocity and the time to achieve

Figure 4.4 Relative Velocity Curves during Stage Separation

5. CONCLUSIONS

To address the significant deviation of high-pressure helium from ideal gas behavior and the cumulative errors associated with conventional cubic EoS, a new corresponding state EoS is proposed based on the intermolecular interaction mechanism and the temperature dependence of molecular forces and molecular volume. On this basis, a transient thermodynamic model is developed using the proposed real-gas EoS, with dedicated modeling strategies formulated for open systems and closed systems. This model is further applied to the case of the interstage high-pressure helium separation process. The main conclusions are as follows:

(1) Within the typical operating temperature range (−30 °C to 120 °C) and pressure range (1–35 MPa) of the interstage separation high-pressure helium system, the proposed real-gas EoS achieves a maximum absolute error below 0.82%. This effectively reduces systematic deviations and significantly improves computational accuracy.

(2) The transient thermodynamic model constructed with the proposed EoS can accurately capture the thermodynamic behavior of fixed-volume open systems, variable-volume open systems, and variable-volume closed systems in the interstage separation process. The

average percentage error compared with experimental data is below 5.2%, thereby validating the effectiveness of the modeling approach in high-pressure gas analysis.

(3) Under heavy-load conditions, where the first and second stages carry 90 t and 120 t, respectively, to satisfy the technical requirements of a separation velocity not lower than 5 m/s and a separation duration of less than 1000 ms, the supply pressure of the gas tank must be no less than 12.5 MPa.

ACKNOWLEDGEMENTS

This research is supported by the National Natural Science Foundation of China (No. 52575071, 52175059), the National Key Research and Development Program of China (No. 2024YFF0505300), and the Shanghai Science and Technology Commission (No. 24YF2745200) through the Rising-Star Program (Yangfan Plan).

NOMENCLATURES

A_1	Effective area of rodless chamber	K	Spring stiffness
A_2	Effective area of rod chamber	m	Mass
a	Molecular interaction strength constant	p	Pressure
B	Damping coefficient	Q	Heat
b	Molecular volume correction constant	T	Temperature
β	Gravitational acceleration correction	T_B	Boyle temperature
c_v	Specific heat capacity	U	Internal energy
$\mathrm{d}m$	Mass flow rate	u	Specific internal energy
E_k	System kinetic energy	v	Specific volume
E_p	System potential energy	V_m	Molar volume
h	Specific enthalpy	W	Work done
I	Degrees of freedom	x	Displacement
Subscripts			
in	Into the system	r	Reduced
out	Out of the system	1	First stage of launch vehicle
c	Critical	2	Second stage of launch vehicle

REFERENCES

[1] S.J. Isakowitz, International reference guide to space launch systems, NASA STI/Recon Technical Report A, vol. 91, pp. 51425, 1991.

[2] J. Lee, Y.-S. Kim, S.-J. Baek, H.S. Jeong, Study of separation mechanism and characteristics of ridge-cut explosive bolts using numerical analysis, International Journal of Aeronautical and Space Sciences, vol. 22, pp. 84–93, 2021.

[3] M. Lucy, R. Hardy, E. Kist, J. Watson, S. Wise, Report on alternative devices to pyrotechnics on spacecraft, 1996.

[4] M. Hihoud, A. Pagès, C. Benoit, F. Claeyssen, S. Sanchez, S. Trémolières, P. Guay, BRUCE – Electromagnetic actuated pin puller, Proc. of the 13th International Conference on New Actuators & 7th International Exhibition on Smart Actuators and Drive Systems, Bremen, Germany, pp. 18–20, 2012.

[5] B. Little, Electrically powered separation nuts, Proc. of the 39th Aerospace Mechanisms Symposium, pp. 7–9, 2008.

[6] W. Tak, M. Lee, B. Kim, Ultimate load and release time controllable non-explosive separation device using a shape memory alloy actuator, Journal of Mechanical Science and Technology, vol. 25, pp. 1141–1147, 2011.
[7] SpaceX, Falcon 9 Launch Vehicle User's Guide, User Manual SpaceX-SPEC-001, Hawthorne, CA, USA, 2021.
[8] E. Hand, Space-science hopes rest on rocket test, Nature, vol. 465, pp. 276–277, 2010.
[9] J.M. McMahon, M.A. Morales, C. Pierleoni, D.M. Ceperley, The properties of hydrogen and helium under extreme conditions, Reviews of Modern Physics, vol. 84, pp. 1607–1653, 2012.
[10] R.J. Thomas, R. Dutta, P. Ghosh, K. Chowdhury, Applicability of equations of state for modeling helium systems, Cryogenics, vol. 52, pp. 375–381, 2012.
[11] J.O. Valderrama, The state of the cubic equations of state, Industrial & Engineering Chemistry Research, vol. 42, pp. 1603–1618, 2003.
[12] Redlich, J.N.S. Kwong, On the thermodynamics of solutions. V. An equation of state. Fugacities of gaseous solutions, Chemical Reviews, vol. 44, pp. 233–244, 1949.
[13] G. Soave, Equilibrium constants from a modified Redlich–Kwong equation of state, Chemical Engineering Science, vol. 27, pp. 1197–1203, 1972.
[14] D.-Y. Peng, D.B. Robinson, A new two-constant equation of state, Industrial & Engineering Chemistry Fundamentals, vol. 15, pp. 59–64, 1976.
[15] A.J. Schultz, D.A. Kofke, Virial equation of state as a new frontier for computational chemistry, The Journal of Chemical Physics, vol. 157, 2022.
[16] B.I. Lee, M.G. Kesler, A generalized thermodynamic correlation based on three-parameter corresponding states, AIChE Journal, vol. 21, pp. 510–527, 1975.
[17] W.G. Chapman, G. Jackson, K.E. Gubbins, Phase equilibria of associating fluids, Molecular Physics, vol. 65, pp. 1057–1079, 1988.
[18] A. Alanazi, M. Ali, S. Bawazeer, N. Yekeen, H. Hoteit, Evaluation of cubic, PC-SAFT, and GERG2008 equations of state for accurate calculations of thermophysical properties of hydrogen-blend mixtures, Energy Reports, vol. 8, pp. 13876–13899, 2022.
[19] S.B. Kiselev, D.G. Friend, Cubic crossover equation of state for mixtures, Fluid Phase Equilibria, vol. 162, pp. 51–82, 1999.
[20] R. Tao, Y. Yin, X. Liu, et al., Novel corresponding states principle equation for real hydrogen under ultra-high pressure considering molecular association, Journal of Mechanical Science and Technology, 2025, pp. 1–13.
[21] R. Tao, Y. Yin, S. Zhu, et al., Performance evaluation and experimental validation of high-pressure pneumatic interstage separation system for reusable launch vehicles considering real gas polytropic process, Aerospace Science and Technology, 2025, 111080.
[22] M. Clarke, et al., Project Columbiad: Mission to the Moon. Book 1: Executive Summary. Vol. 1: Mission trade studies and requirements. Vol. 2: Subsystem trade studies and selection, NASA Technical Report, NAS 1.26:192019, 1992.

Biographies

Ruiyao Tao is a PhD student in the School of Mechanical Engineering, Tongji University, Shanghai, China. Her research interests focus on ultra-high-pressure gas characteristics and flow control properties.

Yaobao Yin is currently a Professor in the School of Mechanical Engineering, Tongji University. He received his Ph.D. from Saitama University, Japan. His main research fields include high-speed aerodynamic control and fluid control in extreme environments, fundamental theories of hydraulics.

Naiping Gao is currently a Professor in the School of Mechanical Engineering, Tongji University. He received his Ph.D. from The Hong Kong Polytechnic University. His main research fields include ventilation and thermal issues in buildings and underground spaces, efficient utilization of low- and medium-temperature thermal energy, and clean combustion of natural gas.

Pengfei He is a Professor in the School of Aerospace Engineering and Applied Mechanics, Tongji University. His research focuses on composite mechanics and computational mechanics, applying molecular dynamics and multiscale modeling to study the mechanical and transport properties of advanced materials such as ionomer membranes, carbon nanotubes, graphene composites, and nanostructured alloys.